Sputtered tungsten nitride films as pseudocapacitive electrode for on chip micro-supercapacitors

Saliha Ouendi, Kevin Robert, Didier Stiévenard, Thierry Brousse, Pascal Roussel, Christophe Lethien

▶ **To cite this version:**

Saliha Ouendi, Kevin Robert, Didier Stiévenard, Thierry Brousse, Pascal Roussel, et al.. Sputtered tungsten nitride films as pseudocapacitive electrode for on chip micro-supercapacitors. Energy Storage Materials, 2019, 20, pp.243-252. 10.1016/j.ensm.2019.04.006 . hal-02187904

HAL Id: hal-02187904
https://hal.science/hal-02187904

Submitted on 26 Jan 2021

HAL is a multi-disciplinary open access archive for the deposit and dissemination of scientific research documents, whether they are published or not. The documents may come from teaching and research institutions in France or abroad, or from public or private research centers.

L'archive ouverte pluridisciplinaire **HAL**, est destinée au dépôt et à la diffusion de documents scientifiques de niveau recherche, publiés ou non, émanant des établissements d'enseignement et de recherche français ou étrangers, des laboratoires publics ou privés.

Accepted Manuscript

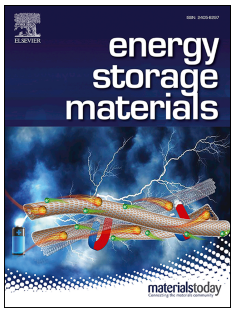

Sputtered tungsten nitride films as pseudocapacitive electrode for on chip micro-supercapacitors

Saliha Ouendi, Kevin Robert, Didier Stievenard, Thierry Brousse, Pascal Roussel, Christophe Lethien

PII: S2405-8297(19)30201-6

DOI: https://doi.org/10.1016/j.ensm.2019.04.006

Reference: ENSM 701

To appear in: *Energy Storage Materials*

Received Date: 8 February 2019

Revised Date: 1 April 2019

Accepted Date: 6 April 2019

Please cite this article as: S. Ouendi, K. Robert, D. Stievenard, T. Brousse, P. Roussel, C. Lethien, Sputtered tungsten nitride films as pseudocapacitive electrode for on chip micro-supercapacitors, *Energy Storage Materials* (2019), doi: https://doi.org/10.1016/j.ensm.2019.04.006.

This is a PDF file of an unedited manuscript that has been accepted for publication. As a service to our customers we are providing this early version of the manuscript. The manuscript will undergo copyediting, typesetting, and review of the resulting proof before it is published in its final form. Please note that during the production process errors may be discovered which could affect the content, and all legal disclaimers that apply to the journal pertain.

ACCEPTED MANUSCRIPT

Sputtered tungsten nitride films for on chip micro-supercapacitors based on pseudocapacitive material for powering miniaturized IoT devices

Saliha Ouendi[1,2], Kevin Robert[1,2], Didier Stievenard[1,2], Thierry Brousse[2,3], Pascal Roussel[4] and Christophe Lethien[1,2*]

Corresponding author: christophe.lethien@univ-lille.fr

[1]Institut d'Electronique, de Microélectronique et de Nanotechnologies (IEMN), Université de Lille, CNRS, Centrale Lille, ISEN, Université de Valenciennes, UMR 8520 - IEMN, F-59000 Lille, France

[2]Réseau sur le Stockage Electrochimique de l'Energie (RS2E), CNRS FR 3459, 33 rue Saint Leu, 80039 Amiens Cedex, France

[3]Institut des Matériaux Jean Rouxel (IMN), CNRS UMR 6502 – Université de Nantes, 2 rue de la Houssinière BP32229, 44322 Nantes cedex 3, France

[4]Unité de Catalyse et de Chimie du Solide (UCCS), Fédération Chevreul, Université de Lille, CNRS, Centrale Lille, ENSCL, Université d'Artois, UMR 8181 – UCCS, F-59000 Lille, France

ACCEPTED MANUSCRIPT

ACCEPTED MANUSCRIPT

Acknowledgment

This research is financially supported by the ANR within the DENSSCAPIO project (ANR-17-CE05-0015-02). The authors also want to thank the French network on electrochemical energy storage (RS2E) for the financial support. The French RENATECH network is greatly acknowledged for the use of microfabrication facilities. Associated Professor Dr Christophe Lethien wants to thank Professor Thierry Brousse and the “Institut des Matériaux de Nantes” for welcoming him as a visiting professor in 2018. Jean Louis Codron and Xavier Wallart are greatly acknowledged for the XPS measurements.

ACCEPTED MANUSCRIPT

ACCEPTED MANUSCRIPT

Sputtered tungsten nitride films as pseudocapacitive electrode for on chip micro-supercapacitors

ABSTRACT: Micro-supercapacitors, a class of miniaturized electrochemical capacitors, are an attractive solution to power smart and connected sensors for Internet of Thing (IoT) applications. Unfortunately, to propose on chip micro-supercapacitors with high technological readiness level, the deposition of electrode materials on large-scale substrate is challenging from microelectronic industry point of view. To fulfill the IoT needs and semiconductor industry requirements, the sputtering deposition of transition metal nitride was investigated in the framework of this paper. Bi-functional tungsten nitride films were sputtered on silicon wafer and were investigated both as a current collector and as an electrode material. Atomic Force Microscopy technique was used to evaluate the specific surface of the sputtered films. 7.9 µm-thick W_2N films exhibits a specific surface of 75 cm^2 per cm^2 footprint area and thus it exhibits capacitance values up to 0.55 $F.cm^{-2}$ and more than 700 $F.cm^{-3}$ in 1M KOH aqueous electrolyte.

KEYWORDS: tungsten nitride, pseudocapacitance, sputtering, AFM, micro-supercapacitor

Graphical abstract

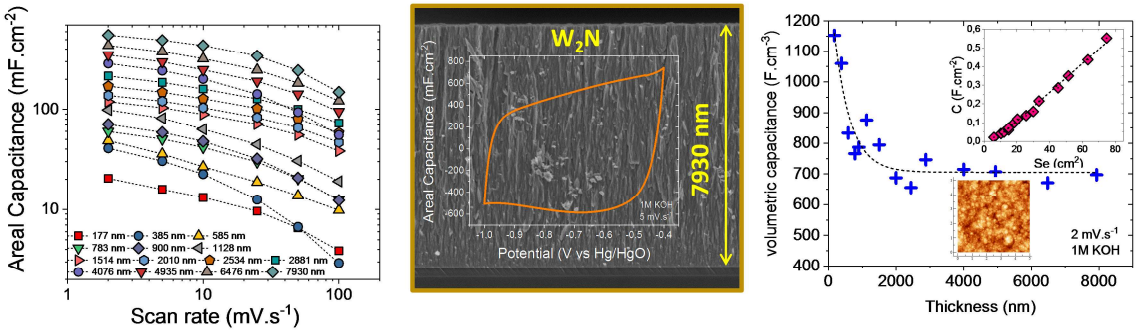

ACCEPTED MANUSCRIPT

RESEARCH HIGHLIGHTS:

- Fine optimization of W_2N pseudocapacitive films deposited by sputtering on silicon wafer for on chip micro-supercapacitors
- Determination of the specific surface of thin films based on AFM imaging technique: specific surface up to 75 cm^2 per cm^2 is evaluated for 7.9-µm thick W_2N film.
- Improvement of the film capacitance: the areal capacitance is significantly increased with thicker layers (7.9 µm-thick) up to 0.55 $F.cm^{-2}$ while maintaining a high volumetric capacitance (700 $F.cm^{-3}$) in 1M KOH electrolyte.

ACCEPTED MANUSCRIPT

INTRODUCTION

Internet of Things (IoT) is burgeoning to exchange data between portable, smart and connected devices [1,2]. Such electronic devices embed various sensors which could be controlled remotely across existing network structure, thus creating opportunities for bridging hardware and software applications in order to design efficient, accurate, self-powered and maintenance-free systems with limited human intervention. Energy scavenging / harvesting technologies are widely investigated for IoT devices to produce self-powering systems with the harvesting from thermal, mechanical or solar energy from the environment and the conversion into electricity. Unfortunately, the intermittence and instability of such resources impose the use of energy storage technologies compatible with the desired application. Miniaturized sensor nodes are required within IoT network for health, environmental or industrial monitoring, drug delivery (*in vivo* application), transportation, wearable personal electronics, radio frequency identification systems. However, it is still challenging to drive these small and connected devices due to the lack of performing and reliable energy storage devices. The miniaturization of different type of electrochemical energy storage (EES) technologies is widely investigated since several years in order to produce efficient EES devices. Micro-supercapacitors [3] (MSC), a class of miniaturized electrochemical capacitors [4], are an attractive solution to power small and connected sensors: nevertheless, the energy density of MSCs is very low and should be improved while keeping the power density and cycling ability high. Recently, carbon based MSC have been fabricated on silicon wafer using semiconductor industrial processes, such as collective microfabrication techniques. MSC are one of the best tradeoff between energy and power densities[5]. To further improve the energy performance of MSC while keeping the power capability and the cycling ability at the highest level, pseudocapacitive materials [6][7] are interesting candidates. Electrodeposited thin films such as MnO_2 or RuO_2 have been investigated in the last few years as efficient electrodes for MSC [8–11]. While MSC are studied since more than 18 years [12], the technological readiness level stays at the lab scale and no industrial products are commercially available. One of the technological barrier is the deposition of active materials (> 5 µm-thick electrode)

using microelectronic equipment, in particular, vapor deposition techniques seem to be really attractive from an industrial point of view. On the one hand, in the semiconductor industry, it is very common to use molecular beam epitaxy or metal organic chemical vapor deposition technique to produce epilayers for electronic, optoelectronic or memory applications. Physical Vapor Deposition techniques such as sputtering or thermal evaporation are also widely used for depositing dense, compact and thin metallic contact layers. On the other hand, for fast electrochemical energy storage application, the electrodes of electrochemical capacitors need to be porous, generally made from transition metal oxides (MnO_2, RuO_2…) or they hydrated phases. Taking into account these two considerations, the first issue is the deposition of porous thin film electrodes for MSC based on large-scale deposition technique. However, the pseudocapacitive material deposited for such purpose must exhibit significant capacitance value, good electrical conductivity and high cycling ability.

Contrary to the widely studied nanoporous carbon or oxides electrodes, there are only few papers focused on nitride based electrochemical capacitors (EC) although, B.E Conway and coworkers [13] demonstrated in 1988 the potential capabilities of molybdenum nitride material acting as an efficient electrode for EC. Transition metal nitrides (TMN) are considered as an important class of materials in many domains (electronics, drilling equipment, catalyst and electrochemistry) due to their high chemical resistance against corrosion, their impressive hardness, their excellent electrical conductivity and their high melting points [14–16]. TMN are investigated recently as electrode materials for Li-ion batteries as well as lithium diffusion barrier in micro-battery [17]. We summarize in the **table 1** the main studies performed on transition metal nitride for EC and MSC.

Since the pioneer work from P. Kumta and coworkers [18] in 2006, vanadium nitride (VN) has been investigated as a promising material for supercapacitors based on the multiple oxidation states of the vanadium cation. High capacitance close to 1340 $F.g^{-1}$ in KOH (1 M) at 2 $mV.s^{-1}$ has been reported [18] for nanosized VO_xN_y based electrode. During the last decade, several TMN (TiN, NbN, Mo_2N, RuN….) have been proposed [19–24] as efficient pseudocapacitive electrodes for SC. Among all these compounds, vanadium nitride is one of the most studied TMN. It was evaluated either as bulk

composite electrode based on VN powder [18] or as thin film electrode [25]. VN – carbon nano fibers composite electrodes[26] have shown impressive capacitance values (up to 600 $mF.cm^{-2}$) in 3M KOH. Such composite electrode is very useful for wearable applications but does not seem to be an attractive solution for micro-supercapacitor due to the synthesis process which is non-compatible with semiconductor industry.

TiN is another promising TMN for EC or MSC: thin films deposited by sputtering [24] or TiN nanowires [27] have been envisioned as interesting electrode materials in KOH or H_2SO_4 aqueous electrolytes (see **table 1**). Mo_xN_y, the first TMN proposed by B. Conway and coworkers [13], is widely studied by many research groups [21,22,28] with different performance depending on the electrode morphology (film, powder) and on the synthesis procedure (sputtering, temperature-programmed reaction).

Among the existing TMN, tungsten nitride (group VI) is rarely studied as an electrode material for electrochemical capacitor [19,29–32], although such TMN exhibits a high electrical conductivity. Combining interesting capacitance values with high electrical conductivity in the same material is very challenging. Here we demonstrate the deposition of bi-functional tungsten nitride films on Si_3N_4 coated silicon wafer. The strategy used to prepare thick W_xN_y electrode (> 5 µm) deposited by magnetron sputtering technique is reported. Structural, morphological and electrochemical properties are carefully investigated in order to optimize the growth of high performance tungsten nitride electrodes for micro-supercapacitor electrodes. Atomic Force Microscopy (AFM) technique is used to investigate the relationship between the specific surface of sputtered films with the electrochemical capacitance measured in aqueous electrolyte. AFM measurements reveal that a 7.9 µm-thick W_2N film exhibits 75 cm^2 per cm^2 specific area. The areal capacitance of such thick W_2N film reaches 0.55 $F.cm^{-2}$ / 700 $F.cm^{-3}$ in 1M KOH. To the best of the authors' knowledge, this value represents the best capacitance published up now for tungsten nitride electrodes and more generally for transition metal nitride films.

METHODS

Sputtering deposition of tungsten nitride thin films

Prior to the deposition of VN thin films, a highly dense Si_3N_4 layer (300 nm) was deposited by low pressure chemical vapor deposition technique (LP CVD) at 800 °C (flow rates: 60 sccm for NH_3 and 20 sccm for SiH_2Cl_2) on the top of the silicon wafer in order to prevent the etching of this substrate by the aqueous electrolyte (KOH and LiOH) used in electrochemical experiments. Tungsten nitride thin films were afterward deposited by reactive magnetron sputtering (Ar / N_2) from a pure 4" tungsten target (99.9 %) using a CT200 Alliance Concept reactor. Before the deposition, the pressure was kept below 10^{-6} mbar and the target-substrate distance was fixed at 6 cm. During the deposition, power density, pressure and argon flow rate were fixed, respectively, at 1.3 $W.cm^{-2}$, 2.5 x 10^{-2} mbar and 28 sccm, while nitrogen flow rate, temperature and deposition time were tuned to find the best performance.

Characterizations of the tungsten nitride thin films

Electrical measurements were performed by Foucault current using a Semilab WT 2000PVN contactless equipment. In this purpose, the thin films were deposited on a high resistivity silicon wafer (R > 5000 ohm.cm). A Zeiss Ultra 55 scanning electron microscope (SEM) was used to determine the morphology (cross section and top view analyses) of the films (thickness).

Structural properties were examined by X-ray diffraction using a Rigaku Smartlab diffractometer equipped with a 9 kW rotated anode. For room temperature experiments, a double Ge (100) monochromator equipped with 0D detector was used with (pure $K_{\alpha,1}$, λ = 1.54056 Å), while for high temperature *in-situ* study, a Bragg-Brentano configuration equipped with a 1D DTEX detector was preferred (average $K_{\alpha1,2}$ radiation, λ = 1.5418 Å)) to speed up the acquisition. In this last configuration, a 2° offset of the substrate was applied to avoid detector saturation due to the high intensity of the (100) silicon peak. JANA 2006 software was used to refine the cell parameters [33].

Surface analyses were performed by X-Ray Photoelectron Spectroscopy using a Physical Electronics type 5600 equipment. All the spectra were fitted with the Multipak ECSA software: peak deconvolution was achieved with asymmetric Gaussian-Lorentz functions and a Shirley background was applied. W *4f*

spectra of the sputtered films were fitted with a *4f* 7/2 – *4f* 5/2 doublet separation of 2.17 eV and with area ratios of 4:3. The film quantification was performed on the survey and the high-resolution spectra (W *4f*, N *1s* and O *1s* core levels) using the CasaXPS software. Only the values extracted from the high-resolution spectra were used.

AFM (Atomic Force Microscope) Dimension 3000 (Bruker) was used in intermittent contact mode with antimony doped Si cantilever (resistivity : 0.01 – 0.025 Ohm.cm, frequency resonance ranging from 130 to 250 kHz –with a constant stiffness k ~ 48 $N.m^{-1}$) to determine the average roughness and the surface morphology of the VN films (WSxM 5.0 software) [34]. Taking advantage of the free software Gwyddion, by P. Klapetek, D. Necas and C. Anderson (version 2.45, 2016) for the analysis of the AFM images, we determined the projected length L_p of the column/pillar, i.e. the total perimeter of the columns measured by the projection of the pillar boundary on an horizontal plane which position was adjusted in order to get a maximum value for L_p i.e. to avoid a coalescence phenomenon (in such a case, the software does not discriminate the top of the columns but detects aggregates : L_p is therefore underestimated). As the surface analysis could depend on its location across a 3 inches silicon coated wafer, we performed measurements on the four quarter of the wafers, and in each quarter, the AFM scan sizes were 3 x 3, 4 x 4 and 5 x 5 μm^2. So, all the data (roughness and L_p) were averaged over 12 measurements and the dispersion of the measured roughness and L_p, for each average, was between 3 to 10 %. Assuming a cylindrical shape of the columns, the specific surface area S_e of the columns was deduced from L_p times the film thickness. The surface values are given for an equivalent top surface of 1 cm^2. This approach could underestimate the exact value of the developed surface since the columns have not a perfect cylindrical shape but contain some additive 3D features. Nevertheless, it allowed determining the evolution of S_e versus the growth conditions of the film.

The electrochemical analyses of the thin films were carried out by cyclic voltammetry with a VMP3 potentiostat / galvanostat (Biologic) using a conventional three-electrode setup in 1M KOH or LiOH

(0.1M, 0.5 and 1M) aqueous electrolytes. The reference and the counter electrodes were Hg/HgO and a platinum wire, respectively. The tested samples sandwiched between the bottom and the top parts of a Biologic flat cell. The tested area were delimited by an O-ring (0.4 cm^2).

ACCEPTED MANUSCRIPT

RESULTS AND DISCUSSION

Structural analyses are reported in **figure 1**. X-Ray diffraction patterns confirm the formation of tungsten nitride (W_xN_y) thin films when nitrogen is used as a reactive gas inside the sputtering reactor. In all the diffractograms **(figure 1a)**, the peak at 2θ = 33 ° corresponds to the λ/2 contribution of the (100) silicon substrate when the substrate is perfectly aligned, i.e. in our case, in the high resolution configuration used at RT. For pure W film (N_2 = 0 sccm), two Bragg peaks are identified in the diffractogram. While the strong peak at 2θ = 40 ° is attributed to the (110) diffraction plane of the cubic metallic tungsten (047-1319 pdf file), the peak at 2θ = 36 ° matches with the (200) Bragg plane of the same metal. When nitrogen is mixed with argon within the sputtering chamber, three peaks are clearly observed in each diffractograms at 2θ ~ 37°, 2θ ~ 43° and 2θ ~ 62° respectively. According to the position of these Bragg peaks, only W_2N or $W_{0.62}NO$ cubic phases (025-1257 or 025-1254 pdf files) can match with the diffractograms taking into account a shift of all the reflection peaks towards lower 2θ values probably due to stress issues. Such observations are classically reported for sputtered transition metal nitride films [35,36] exhibiting compact / dense morphology owing to the atomic peening and adatoms diffusion effects [37]. High energetic particles bombard the film surface leading to the insertion of excess atoms into interstitial sites, in turn leading to the expansion of the lattice parameter. We could not fit the diffractograms with the tungsten nitride (WN, 025-1256 pdf file) or $W_{0.75}NO$ (025-1255 pdf file) crystallographic structures thus indicating an atomic concentration of tungsten below 70 % in all the sputtered thin films. A steady increase of the nitrogen flow during the sputtering process leads to a shift of the (111) Bragg peak toward lower 2θ value (**figure 1b**) indicating an expansion of the lattice parameter due to excess of N atoms [35,36]: the higher the nitrogen concentration, the higher the lattice parameter (**figure 1c – right axis**). Such XRD analysis is essential to determine the crystallographic structure of sputtered tungsten nitride films but, regarding the position of the Bragg peaks, only W_2N or $W_{0.62}NO$ phases could fit with the experimental diffractogramms when the nitrogen flow rate is limited to 11 sccm in the sputtering gas. To dismiss one phase regarding the other, the quantification of the elements within the tungsten nitride film is essential. The film

composition is plotted in **figure 1c (left axis)** and the quantification is determined from XPS spectra. The plots of the atomic ratio reported in **figure 1c** clearly show the progressive decrease of the W / N ratio when the N_2 flow rate is increased following the same conclusion already reported for sputtered tungsten nitride films [35], and confirming the formation of W_2N phase instead of $W_{0.62}NO$ compound (W / N ~ 2). The progressive shift of the (111) Bragg peak (at ~ 37°) toward low 2θ theta value when nitrogen concentration in the plasma increases tends to converge to the (100) peak of the WN theoretical pattern at ~ 35 ° (025-1256 pdf card). Nevertheless, based on our sputtering conditions, the N_2 concentration in the plasma is too low to form the WN structure.

The electrical conductivity was studied as a function of the N_2 flow rate (**figure 1d**). Not surprisingly, the higher the nitrogen concentration, the lower the electrical conductivity. The electrical conductivity shifts from 33 000 $S.cm^{-1}$ for pure W film down to 220 $S.cm^{-1}$ when the N_2 flow rate is close to 11 sccm. Such measurement clearly supports the pertinence of the study since W_2N films are intended to be used as a bifunctional material for micro-supercapacitor, i.e. as a current collector and an electrode material.

XPS analyses are depicted in **figure 1e** (N *1s* and W *4f* core levels) and **figure SI1** (O *1s* and C *1s* core levels). These surface analyses allow studying the chemical bonding configuration. The sputtered tungsten nitride films are exposed to air before XPS measurements. Consequently, the survey scan reveals the presence of W, N and O elements with carbon contamination (not shown here). A shift of the XPS peaks is observed in the W *4f* energy region as the nitrogen concentration increases during the sputtering process. Four peaks are classically observed in the W *4f* spectra. At low binding energy (30 – 35 eV), two peaks are attributed to the W *4f* 7/2 and W *4f* 5/2 doublet while the two other peaks (ΔE = 2.17 eV) in the high energy region (35 – 40 eV) match with the ones of WO_3 [35,38,39], confirming the presence of tungsten tri-oxide in all the sputtered tungsten nitride films. Not surprisingly, the peaks in the low energy region (31 – 35 eV) shift as a function of the nitrogen flow rate. For pure W film, the W *4f* peaks are located at 31.5 and 33.8 eV respectively. When the nitrogen

partial pressure increases, the W *4f* peaks progressively shift to 33.0 and 35.2 eV respectively: such binding energies are typically reported for W_2N compound [35,39,40]. The N *1s* core level spectrum reported in **figure 1c** confirms this assumption with a W-N binding energy close to 397.2 eV (main contribution) typically observed for W_2N. No additional peaks are observed in the N *1s* core level spectra at an energy level lower than 398 eV thus demonstrating the non-oxidized form of the transition metal nitride films[24,41]. As no peaks are assigned to W_xO_y oxide in the XRD patterns, we suppose to the formation of sputtered W_2N films as a "the core" material surrounded by a very thin "shell" of amorphous or crystallized tungsten oxide (WO_3). Further investigations are needed to confirm this assumption.

The electrochemical investigations are reported in **figure 2**. As shown in **table 1**, many TMN exhibit high capacitance when cycled in aqueous electrolyte containing OH^- ions [18,31,42,43]. Not surprisingly, the CV of pure W film does not show any redox peaks when cycled in 1M KOH (**figure 2a**). The CVs of W_2N films deposited with different N_2 flow rates are shown in **figure SI2** and **figure 2b** when tested in 1M KOH electrolyte. The CV at N_2 = 3 sccm exhibits a rectangular shape at low sweep rate which becomes slightly distorted at higher sweep rate (**figure SI2**). When the N_2 flow rate is increased, the CVs exhibits quasi-rectangular shapes for N_2 = 5 and 7 sccm (**figure SI2**). At higher N_2 partial pressures (N_2 = 9 or 11 sccm), most of the CVs – at low and high sweep rates – are distorted (**figure SI2**). Nevertheless, an anodic irreversible process is observed when the W_2N film is cycled up to -0.3 V vs Hg/HgO (**figure 2b, blue curve**). Such process could be ascribed to a dissolution or to a passivation (change of the film surface) of W_2N as observed by A. Morel *et al* on sputtered VN films [43]. This phenomenon is confirmed in **figure 2c** (**blue curve**) where a fade in capacitance is observed during the first 1600 cycles when the W_2N film is cycled in 1M KOH electrolyte between -1 V and -0.3 V vs HgO. Moving from -0.3 V to lower potential (-0.4 V vs Hg/HgO) allows limiting this anodic irreversible process (**figure 2b, red curve**) and consequently, improving the retention of the capacitance (**figure 2c, red curve**) close to 100 % with no fade over 1600 cycles. To clearly compare the effect of the N_2 flow rate onto the capacitance of the films, the volumetric capacitances are plotted as a function of the

sweep rate by normalizing the areal capacitance with the film thickness measured by SEM (**figure 2d**). The volumetric capacitance is used here for comparison purpose only since it is not the suitable metric for micro-supercapacitor applications [3]. At 2 $mV.s^{-1}$, the film deposited at N_2 = 7 sccm exhibits quite an impressive volumetric capacitance higher than 1000 $F.cm^{-3}$. Such high value, confirms the pseudocapacitive nature of the W_2N films. It is typically 2.5 times higher than the value [5] of carbon based thin film electrodes (Carbide Derived Carbon CDC, 400 $F.cm^{-3}$) tested in 1M H_2SO_4 aqueous electrolyte and 2 times higher than the value of MXene electrodes (500 $F.cm^{-3}$) tested in 1M KOH [44,45]. At lower N_2 flow rate, the volumetric capacitance is lower confirming the use of N_2 = 7 sccm as the best candidate. To confirm the role of OH^- anions in the charge storage process, we perform some electrochemical analysis of the W_2N deposited at N_2 = 7 sccm in LiOH based electrolyte with different concentrations (from 0.1M to 1M). As expected, the CVs at 10 $mV.s^{-1}$ exhibit rectangular shape thus confirming the pseudocapacitive nature of the W_2N films (**figure 2e**). The lowest concentrated LiOH electrolyte induces lower areal capacitance (**figure 2f**) and the capacitance at 1M LiOH is at the same level of magnitude than the capacitance measured in 1M KOH confirming the role of hydroxyl ions in the charge storage mechanism of W_2N films.

The electrochemical performance of the W_2N films deposited at room temperature (RT) was studied in the previous paragraph where the pseudocapacitive behavior of tungsten nitride thin films was highlighted. Nevertheless, it was not possible to keep a high areal or volumetric capacitance at high sweep rate. To reach this goal, the electrical conductivity has been improved following the same approach that the one published by C. Lethien and coworkers for vanadium nitride thin films [42]. As a matter of fact, the deposition of W_2N films was achieved on silicon wafer at high temperature, i.e. by maintaining the temperature of the substrate at a high value during the deposition. The electrical and electrochemical analyses are reported in **figure 3**. The electrical conductivity is shown in **figure 3a** where an increase of the electrical conductivity is observed as the deposition temperature is increased from RT to 700 °C. Such improvement of the film conductivity is due to a film densification and / or a release of the trapped nitrogen into the interstitial sites outside the W_2N structure [36]. Such

hypothesis is confirmed by XRD patterns reported in **figure SI3** where a shift of the Bragg peaks towards the higher two theta values is observed, thus leading to a decrease of the lattice parameter. Regarding the film morphology depicted in **figure 3b**, the progressive film densification is evidence as expected with an increase of the deposition temperature. The **figures 3c** and **3d** report on the evolution of the cyclic voltammograms obtained with different electrochemical windows, between -0.4 V and -1.3 V vs Hg/HgO (**figure 3c**) and between -1.0 V and -0.2 V vs Hg/HgO (**figure 3d**). As previously observed for sputtered vanadium nitride films [42,43] and for sputtered W_2N deposited at RT, large irreversible cathodic and anodic processes are depicted. Such irreversible processes, confirmed by electrochemical impedance spectroscopy (**figure 3e**) are not suitable for long term cycling where not only the coulombic efficiency of the film is impaired but also the capacitance retention. When the measurement is performed outside the electrochemical stability window of the electrode, the Nyquist plot changes towards a non-capacitive behavior (non-vertical line) at low frequency. The CVs of the sputtered W_2N film deposited at 600 °C are shown in **figure 3f**. The CVs seem to be less distorted when cycled at high sweep rate but the film capacitances, normalized by the thickness (i.e. the volumetric capacitance), are lower than the capacitance values reached at RT (**figure 3g**). The capacitance retention of W_2N films is depicted in **figure 3h** over 10 000 cycles at 50 $mV.s^{-1}$. Not surprisingly, long term cycling do not degraded the electrochemical performance which demonstrate the interesting potential of tungsten nitride film for micro-supercapacitor applications. Film densification, resulting from better adatoms diffusion occurring during the sputtering process, decreases the inter-columnar spacing and limits the accessible surface for the liquid electrolyte. Consequently, the capacitance value reaches a steady state after several hundredth of cycles as shown in **figure 3h**. Hence, there is no added value to deposit W_2N film at high temperature especially with regards to micro-supercapacitor applications. Furthermore, from industrial and environmental points of view, the development of fast deposition process at room temperature is clearly an attractive solution to promote the fast technological transfer towards pilot production line.

Nevertheless, the technological readiness level (TRL) of micro-supercapacitors stays at a low level, i.e. at the lab scale, due to the difficulty to achieve the homogeneous deposition of active materials on large sale substrate limiting the collective fabrication of many miniaturized energy storage devices on silicon wafer. Indeed, vapor deposition techniques are widely developed in the semiconductor industry and sputtering facilities are the main deposition tools used for the development of commercially off the shelf lithium based micro-batteries [46,47]. A way to improve the performance of on chip micro-supercapacitors is to increase the material mass loading of sputtered W_2N electrode. To reach this goal, the thickness of the W_2N films was progressively increased by tuning the deposition time (**figure 4a**). The cross section imaging by SEM is reported in **figure SI4a-d**. As expected, based on the optimized deposition parameters, the columnar growth is maintained when the film thickness moves from 177 up to 7930 nm. The corresponding AFM top view images are reported in figure **SI4e-h**. As the W_2N thickness increases, the morphology of the film changes slowly, from grains (associated with the top of the columns) with homogeneous size (**figure SI4e**) to grains with small and bigger sizes (**figure SI4h**), concomitantly leading to a decrease of the projected length L_p. Indeed, the bigger the grain size, the smaller L_p. Assuming a homogeneous filling of a square area (scanned area with side dimension = a) with numerous circles (diameter = D), the sum of the perimeters of the circles (i.e. L_p in our case) is given by $L_p = \pi a^2 / D$. Consequently, L_p decreases when D increases. As shown in **figure 4b**, the average roughness of the W_2N films increases from 1.5 to 18 nm as the thickness of the films moves from 177 to 7930 nm. This is in agreement with the maximum height of the grains which varies from typically 55 nm to 180 nm, as illustrated in **figures SI4e-h**. For thicker W_2N films, the roughness varies slowly, meaning that the roughness is less and less sensitive to the thickness. Similar conclusions could be done for L_p that is getting less thickness-dependent as depicted in **figure 4c**. Typically, L_p decreases from 34 to 9 µm as the WN thickness moves from 177 to 7930 nm. A steady state of the L_p value is then observed for thickness greater than 2000 nm. As the thickness reaches such value, the morphology of the W_2N columns varies slowly giving rise to the observed conclusions for the roughness and the projected length L_p. According to the variation of L_p, S_e increases from

typically 6 to 75 cm^2 per cm^2. This linear behavior is interesting since it shows that the growth is homogeneous and it is therefore possible to increase S_e (and therefore the capacitance) simply by increasing the thickness.

While AFM top surface analyses clearly demonstrate the improvement of the specific surface, the electrochemical performance have to be evaluated in 1M KOH in order to highlight the pertinence of our approach and to find the potential limitations. The CVs at 5 $mV.s^{-1}$ of numerous samples exhibiting different thicknesses are reported in **figure 4d** and **4e**: all the samples were tested in 1M KOH between -1 and -0.4 V vs Hg/HgO. The cyclic voltamogramms of all the samples exhibit a quasi-rectangular shape characteristic of pseudocapacitive electrodes and the surface capacitance is reported at different sweep rates in **figure 4f**. It can be pointed out a similar shape of all the plots. The thicker the W_2N layer, the higher the surface capacitance of the films. While 177 nm-thick films (**figure 4f**) exhibits a low surface capacitance (20 $mF.cm^{-2}$), the 7930 nm-thick W_2N sample shows a maximum areal capacitance close to 550 $mF.cm^{-2}$ at 2 $mV.s^{-1}$. Regarding the capacitances reported in **table 1**, the value obtained here seems to be one of the highest capacitance value reported up to now for nitride thin films deposited with industrial deposition technique widely developed in semiconductor industry. We observe a good correlation and a linear relationship between the specific surface extracted from AFM measurement and the areal capacitance **(figure 4g)** measured in 1M KOH at 5 $mV.s^{-1}$ demonstrating the pertinence of the methodology that was used to determine the specific surface of thin films by AFM. This is confirmed by electrochemical analysis: for 783 nm-thick W_2N film, C = 58 $mF.cm^{-2}$ which is 1/10 of the capacitance measured for the thicker film (7930 nm). Moreover, the increase in film thickness does not seem to lead to a maximum in the capacitance, even up to 7930 nm and further studies are needed to determine the potential limitation of our strategy. Finally, the volumetric capacitance of the W_2N was reported as a function of the film thickness (**figure 4h**). When the mass loading is very low, the volumetric capacitance is 1150 $F.cm^{-3}$ taking into account a 177 nm-thick film. The capacitance decreases down to 700 $F.cm^{-3}$, which seems to be an equilibrium value, as soon as the thickness is higher than 2000 nm. This interesting value is higher than numerous MXene bulk

electrodes [48]. Nevertheless, as mentioned previously, volumetric capacitance is not the suitable metric for micro-supercapacitors which are surface-dependent device. Indeed, we observe in **figure 4h** the effect of mass loading onto the electrochemical performance when thin or thick layers are deposited as already pointed out by P. Simon and coworkers [49,50]. For MSC applications, the mass loading is generally low and numerous papers report the performance in $F.cm^{-3}$, $mWh.cm^{-3}$ or $W.cm^{-3}$ while several guidelines are published [3,51] on this topic in order to invite the scientific community working on micro-supercapacitor to use surface metrics ($F.cm^{-2}$, $mWh.cm^{-2}$ and $mW.cm^{-2}$).

Conclusion. In this work, we have successfully deposited tungsten nitride films on silicon wafer by magnetron sputtering technique. The films deposited at room temperature have demonstrated the best performance as compared to films deposited at higher temperature. Sputtered W_2N films (up to 7.9 µm-thick) deliver interesting areal (550 $mF.cm^{-2}$) and volumetric capacitances (> 700 $F.cm^{-3}$) , confirming the pseudocapacitive nature of W_2N films. Atomic Force Microscopy has been used to evaluate the specific surface of tungsten nitride thin films. The thicker W_2N film (7.9 µm) exhibits up to 75 cm^2 specific surface per cm^2 footprint area. A linear relationship between the surface capacitance and the measured specific surface was also evidenced. Further investigations are currently on going to increase the film thickness and so the areal capacitance of sputtered tungsten nitride electrodes. Thus the design of new micro-supercapacitors using W_2N electrodes can be envisioned.

Acknowledgments

-see title page

Data availability

The raw/processed data required to reproduce these findings cannot be shared at this time as the data also forms part of an ongoing study.

References.

[1] A. Whitmore, A. Agarwal, L. Da Xu, The Internet of Things—A survey of topics and trends, Inf. Syst. Front. 17 (2015) 261–274. doi:10.1007/s10796-014-9489-2.

[2] L. Atzori, A. Iera, G. Morabito, The Internet of Things: A survey, Comput. Networks. 54 (2010) 2787–2805. doi:10.1016/j.comnet.2010.05.010.

[3] C. Lethien, J. Le Bideau, T. Brousse, Challenges and prospects of 3D micro-supercapacitors for powering the internet of things, Energy Environ. Sci. 12 (2019) 96–115. doi:10.1039/C8EE02029A.

[4] P. Simon, Y. Gogotsi, Materials for electrochemical capacitors, Nat. Mater. 7 (2008) 845–854. doi:10.1038/nmat2297.

[5] P. Huang, C. Lethien, S. Pinaud, K. Brousse, R. Laloo, V. Turq, M. Respaud, A. Demortiere, B. Daffos, P.L. Taberna, B. Chaudret, Y. Gogotsi, P. Simon, On-chip and freestanding elastic carbon films for micro-supercapacitors, Science (80-.). 351 (2016) 691–695. doi:10.1126/science.aad3345.

[6] M. Toupin, T. Brousse, D. Bélanger, Charge storage mechanism of MnO2 electrode used in aqueous electrochemical capacitor, Chem. Mater. 16 (2004) 3184–3190. doi:10.1021/cm049649j.

[7] T. Brousse, D. Bélanger, J.W. Long, To Be or Not To Be Pseudocapacitive?, J. Electrochem. Soc. 162 (2015) A5185–A5189. doi:10.1149/2.0201505jes.

[8] E. Eustache, C. Douard, R. Retoux, C. Lethien, T. Brousse, MnO<inf>2</inf> Thin Films on 3D Scaffold: Microsupercapacitor Electrodes Competing with “bulk” Carbon Electrodes, Adv. Energy Mater. 5 (2015) 3–7. doi:10.1002/aenm.201500680.

[9] A. Ferris, S. Garbarino, D. Guay, D. Pech, 3D RuO2 Microsupercapacitors with Remarkable Areal

Energy, Adv. Mater. 27 (2015) 6625–6629. doi:10.1002/adma.201503054.

[10] M.F. El-Kady, M. Ihns, M. Li, J.Y. Hwang, M.F. Mousavi, L. Chaney, A.T. Lech, R.B. Kaner, Engineering three-dimensional hybrid supercapacitors and microsupercapacitors for high-performance integrated energy storage, Proc. Natl. Acad. Sci. 112 (2015) 4233–4238. doi:10.1073/pnas.1420398112.

[11] E. Eustache, C. Douard, A. Demortière, V. De Andrade, M. Brachet, J. Le Bideau, T. Brousse, C. Lethien, High Areal Energy 3D-Interdigitated Micro-Supercapacitors in Aqueous and Ionic Liquid Electrolytes, Adv. Mater. Technol. 2 (2017) 1700126. doi:10.1002/admt.201700126.

[12] Y.S. Yoon, W.I. Cho, J.H. Lim, D.J. Choi, Solid-state thin-film supercapacitor with ruthenium oxide and solid electrolyte thin films, J. Power Sources. 101 (2001) 126–129. doi:10.1016/S0378-7753(01)00484-0.

[13] T.-C. Liu, W.G. Pell, S.L. Roberson, B.E. Conway, Behavior of Molybdenum Nitrides as Materials for Electrochemical Capacitors, J. Electrochem. Soc. 145 (1998) 1882. doi:10.1149/1.1838571.

[14] M.-S. Balogun, W. Qiu, W. Wang, P. Fang, X. Lu, Y. Tong, Recent advances in metal nitrides as high-performance electrode materials for energy storage devices, J. Mater. Chem. A. 3 (2015) 1364–1387. doi:10.1039/C4TA05565A.

[15] H.O. Pierson, Handbook of refractory carbides and nitrides : properties, characteristics, processing, and applications, Handb. Refract. Carbides Nitrides. (1996) 362. doi:10.1016/B978-081551392-6.50005-2.

[16] B. Gao, X. Li, K. Ding, C. Huang, Q. Li, P.K. Chu, K. Huo, Recent progress in nanostructured transition metal nitrides for advanced electrochemical energy storage, J. Mater. Chem. A. 7 (2019) 14–37. doi:10.1039/c8ta05760e.

[17] J. Freixas, E. Eustache, P. Roussel, C. Brillard, D. Deresmes, N. Nuns, N. Rolland, T. Brousse, C.

Lethien, Sputtered Titanium Nitride: A Bifunctional Material for Li-Ion Microbatteries, J. Electrochem. Soc. 162 (2015) 493–500. doi:10.1149/2.0051504jes.

[18] D. Choi, G.E. Blomgren, P.N. Kumta, Fast and reversible surface redox reaction in nanocrystalline vanadium nitride supercapacitors, Adv. Mater. 18 (2006) 1178–1182. doi:10.1002/adma.200502471.

[19] D. Choi, P.N. Kumta, Synthesis, structure, and electrochemical characterization of nanocrystalline tantalum and tungsten nitrides, J. Am. Ceram. Soc. 90 (2007) 3113–3120. doi:10.1111/j.1551-2916.2007.01873.x.

[20] D. Choi, P.N. Kumta, Synthesis and characterization of nanostructured niobium and molybdenum nitrides by a two-step transition metal halide approach, J. Am. Ceram. Soc. 94 (2011) 2371–2378. doi:10.1111/j.1551-2916.2011.04412.x.

[21] P. Pande, P.G. Rasmussen, L.T. Thompson, Charge storage on nanostructured early transition metal nitrides and carbides, J. Power Sources. 207 (2012) 212–215. doi:10.1016/j.jpowsour.2012.01.028.

[22] A.E.S. Sleightholme, L.T. Thompson, A. Deb, J. Penner-Hahn, A. Djire, P.G. Rasmussen, P. Pande, Pseudocapacitive charge storage via hydrogen insertion for molybdenum nitrides, J. Power Sources. 289 (2015) 154–159. doi:10.1016/j.jpowsour.2015.03.171.

[23] S. Bouhtiyya, R. Lucio Porto, B. Laïk, P. Boulet, F. Capon, J.P. Pereira-Ramos, T. Brousse, J.F. Pierson, Application of sputtered ruthenium nitride thin films as electrode material for energy-storage devices, Scr. Mater. 68 (2013) 659–662. doi:10.1016/j.scriptamat.2013.01.030.

[24] A. Achour, R.L. Porto, M.A. Soussou, M. Islam, M. Boujtita, K.A. Aissa, L. Le Brizoual, A. Djouadi, T. Brousse, Titanium nitride films for micro-supercapacitors: Effect of surface chemistry and film morphology on the capacitance, J. Power Sources. 300 (2015) 525–532.

doi:10.1016/j.jpowsour.2015.09.012.

[25] R. Lucio-Porto, S. Bouhtiyya, J.F. Pierson, A. Morel, F. Capon, P. Boulet, T. Brousse, VN thin films as electrode materials for electrochemical capacitors, Electrochim. Acta. 141 (2014) 203–211. doi:10.1016/j.electacta.2014.07.056.

[26] J. Guo, Q. Zhang, J. Sun, C. Li, J. Zhao, Z. Zhou, B. He, X. Wang, P. Man, Q. Li, J. Zhang, L. Xie, M. Li, Y. Yao, Direct growth of vanadium nitride nanosheets on carbon nanotube fibers as novel negative electrodes for high-energy-density wearable fiber-shaped asymmetric supercapacitors, J. Power Sources. 382 (2018) 122–127. doi:10.1016/j.jpowsour.2018.02.034.

[27] X. Zhou, C. Shang, L. Gu, S. Dong, X. Chen, P. Han, L. Li, J. Yao, Z. Liu, H. Xu, Y. Zhu, G. Cui, Mesoporous coaxial titanium nitride-vanadium nitride fibers of core-shell structures for high-performance supercapacitors, ACS Appl. Mater. Interfaces. 3 (2011) 3058–3063. doi:10.1021/am200564b.

[28] L. Chen, C. Liu, Z. Zhang, Novel [111] oriented γ-Mo2N thin films deposited by magnetron sputtering as an anode for aqueous micro-supercapacitors, Electrochim. Acta. 245 (2017) 237–248. doi:10.1016/j.electacta.2017.05.102.

[29] Y. Zeng, M. Chen, X. Cheng, Y. Tong, M. Yu, L. Hu, X. Lu, Y. Han, F. Cheng, Holey Tungsten Oxynitride Nanowires: Novel Anodes Efficiently Integrate Microbial Chemical Energy Conversion and Electrochemical Energy Storage, Adv. Mater. 27 (2015) 3085–3091. doi:10.1002/adma.201500493.

[30] A. Djire, O.T. Ajenifujah, A.E.S. Sleightholme, P. Rasmussen, L.T. Thompson, Effects of surface oxygen on charge storage in high surface area early transition-metal carbides and nitrides, J. Power Sources. 275 (2015) 159–166. doi:10.1016/j.jpowsour.2014.10.161.

[31] A.M. Glushenkov, O. Kartachova, H. Zhang, X.J. Dai, Y. Chen, Y. Chen, Electrochemical

capacitance of mesoporous tungsten oxynitride in aqueous electrolytes, J. Power Sources. 220 (2012) 298–305. doi:10.1016/j.jpowsour.2012.07.132.

[32] O. Kartachova, A.M. Glushenkov, Y. Chen, H. Zhang, Y. Chen, Bimetallic molybdenum tungsten oxynitride: Structure and electrochemical properties, J. Mater. Chem. A. 1 (2013) 7889–7895. doi:10.1039/c3ta10836h.

[33] V. Petrícek, M. Dušek, L. Palatinus, Crystallographic computing system JANA2006: General features, Zeitschrift Fur Krist. 229 (2014) 345–352. doi:10.1515/zkri-2014-1737.

[34] J.M. Gómez-Rodríguez, I. Horcas, J. Gómez-Herrero, A.M. Baro, J. Colchero, R. Fernández, WSXM : A software for scanning probe microscopy and a tool for nanotechnology , Rev. Sci. Instrum. 78 (2007) 013705. doi:10.1063/1.2432410.

[35] C.C. Baker, S.I. Shah, Reactive sputter deposition of tungsten nitride thin films, J. Vac. Sci. Technol. A Vacuum, Surfaces, Film. 20 (2002) 1699–1703. doi:10.1116/1.1498278.

[36] Y.G. Shen, Y.W. Mai, Effect of oxygen on residual stress and structural properties of tungsten nitride films grown by reactive magnetron sputtering, Mater. Sci. Eng. B Solid-State Mater. Adv. Technol. 76 (2000) 107–115. doi:10.1016/S0921-5107(00)00424-4.

[37] P. Huang, M. Létiche, M. Respaud, B. Chaudret, A. Demortière, K. Brousse, S. Pinaud, L. Buchaillot, P. Simon, P.L. Taberna, B. Daffos, P. Roussel, C. Lethien, Sputtered Titanium Carbide Thick Film for High Areal Energy on Chip Carbon-Based Micro-Supercapacitors, Adv. Funct. Mater. 27 (2017) 1606813. doi:10.1002/adfm.201606813.

[38] Z. Wang, Z. Liu, Z. Yang, S. Shingubara, Characterization of sputtered tungsten nitride film and its application to Cu electroless plating, Microelectron. Eng. 85 (2008) 395–400. doi:10.1016/j.mee.2007.07.017.

[39] Y.G. Shen, Y.W. Mai, D.R. McKenzie, Q.C. Zhang, W.D. McFall, W.E. McBride, Composition,

residual stress, and structural properties of thin tungsten nitride films deposited by reactive magnetron sputtering, J. Appl. Phys. 88 (2000) 1380–1388. doi:10.1063/1.373827.

[40] Y.G. Shen, Y.W. Mai, Q.C. Zhang, D.R. McKenzie, W.D. McFall, W.E. McBride, Residual stress, microstructure, and structure of tungsten thin films deposited by magnetron sputtering, J. Appl. Phys. 87 (2000) 177–187. doi:10.1063/1.371841.

[41] F.H. Lu, H.Y. Chen, XPS analyses of TiN films on Cu substrates after annealing in the controlled atmosphere, Thin Solid Films. 355 (1999) 374–379. doi:10.1016/S0040-6090(99)00454-X.

[42] C. Douard, P. Roussel, F. Blanchard, K. Robert, C. Lethien, T. Brousse, A. Demortière, On Chip Interdigitated Micro-Supercapacitors Based on Sputtered Bifunctional Vanadium Nitride Thin Films with Finely Tuned Inter- and Intracolumnar Porosities, Adv. Mater. Technol. 3 (2018) 1800036. doi:10.1002/admt.201800036.

[43] Y. Borjon-Piron, A. Morel, D. Bélanger, R.L. Porto, T. Brousse, Suitable Conditions for the Use of Vanadium Nitride as an Electrode for Electrochemical Capacitor, J. Electrochem. Soc. 163 (2016) A1077–A1082. doi:10.1149/2.1221606jes.

[44] M.R. Lukatskaya, O. Mashtalir, C.E. Ren, Y. Dall'Agnese, P. Rozier, P.L. Taberna, M. Naguib, P. Simon, M.W. Barsoum, Y. Gogotsi, Cation Intercalation and High Volumetric Capacitance of Two-Dimensional Titanium Carbide, Science (80-.). 341 (2013) 1502–1505. doi:10.1126/science.1241488.

[45] B. Anasori, M.R. Lukatskaya, Y. Gogotsi, 2D metal carbides and nitrides (MXenes) for energy storage, Nat. Rev. Mater. 2 (2017) 16098. doi:10.1038/natrevmats.2016.98.

[46] B. Laïk, I. Ressejac, C. Venet, J.P. Pereira-Ramos, Comparative study of electrochemical performance of commercial solid-state thin film Li microbatteries, Thin Solid Films. 649 (2018) 69–74. doi:10.1016/j.tsf.2018.01.033.

[47] M. Hallot, A. Demortière, P. Roussel, C. Lethien, Sputtered LiMn1.5Ni0.5O4 thin films for Li-ion micro-batteries with high energy and rate capabilities, Energy Storage Mater. 15 (2018) 396–406. doi:10.1016/j.ensm.2018.08.012.

[48] B. Anasori, M.R. Lukatskaya, Y. Gogotsi, 2D metal carbides and nitrides (MXenes) for energy storage, Nat. Rev. Mater. 2 (2017). doi:10.1038/natrevmats.2016.98.

[49] Y. Gogotsi, P. Simon, True Performance Metrics in Electrochemical Energy Storage, Science (80-.). 334 (2011) 917–918. doi:10.1126/science.1213003.

[50] J. Chmiola, C. Largeot, P.L. Taberna, P. Simon, Y. Gogotsi, Monolithic Carbide-Derived Carbon Films for Micro-Supercapacitors, Science (80-.). 328 (2010) 480–483. doi:10.1126/science.1184126.

[51] D. Belanger, W. Sugimoto, A. Balducci, T. Brousse, J.W. Long, Perspective—A Guideline for Reporting Performance Metrics with Electrochemical Capacitors: From Electrode Materials to Full Devices, J. Electrochem. Soc. 164 (2017) A1487–A1488. doi:10.1149/2.0851707jes.

[52] D. Choi, P.N. Kumta, Chemically Synthesized Nanostructured VN for Pseudocapacitor Application, Electrochem. Solid-State Lett. 8 (2006) A418. doi:10.1149/1.1951201.

[53] O. Bondarchuk, A. Morel, D. Bélanger, E. Goikolea, T. Brousse, R. Mysyk, Thin films of pure vanadium nitride: Evidence for anomalous non-faradaic capacitance, J. Power Sources. 324 (2016) 439–446. doi:10.1016/j.jpowsour.2016.05.093.

[54] B. Wei, H. Liang, D. Zhang, Z. Qi, H. Shen, Z. Wang, Magnetron sputtered TiN thin films toward enhanced performance supercapacitor electrodes, Mater. Renew. Sustain. Energy. 7 (2018) 1–9. doi:10.1007/s40243-018-0117-9.

[55] B. Wei, H. Liang, D. Zhang, Z. Wu, Z. Qi, Z. Wang, CrN thin films prepared by reactive DC magnetron sputtering for symmetric supercapacitors, J. Mater. Chem. A. 5 (2017) 2844–2851.

doi:10.1039/c6ta09985h.

[56] G. Mei, H. Liang, D. Zhang, B. Wei, Z. Qi, H. Shen, Z. Wang, Porous CrN thin films by selectively etching CrCuN for symmetric supercapacitors, J. Power Sources. 385 (2018) 39–44. doi:10.1016/j.jpowsour.2018.03.023.

[57] Y. Xie, F. Tian, Capacitive performance of molybdenum nitride/titanium nitride nanotube array for supercapacitor, Mater. Sci. Eng. B Solid-State Mater. Adv. Technol. 215 (2017) 64–70. doi:10.1016/j.mseb.2016.11.005.

[58] L. Le Brizoual, M.A. Soussou, A. Achour, A. Ahmadpourian, T. Brousse, M. Boujtita, M. Chaker, R. Lucio-Porto, A. Arman, M.A. Djouadi, Titanium vanadium nitride electrode for micro-supercapacitors, Electrochem. Commun. 77 (2017) 40–43. doi:10.1016/j.elecom.2017.02.011.

[59] H. Cui, G. Zhu, X. Liu, F. Liu, Y. Xie, C. Yang, T. Lin, H. Gu, F. Huang, Niobium Nitride Nb4N5 as a New High-Performance Electrode Material for Supercapacitors, Adv. Sci. 2 (2015) 1–12. doi:10.1002/advs.201500126.

ACCEPTED MANUSCRIPT

List of the figures and figure caption

Material	Ref	Capacitance	Electrolyte	Thickness	Potential window (V)
Mo_xN	[13]	50 $mF.cm^{-2}$	0.5M H_2SO_4	15 µm	0.6
VN	[18]	1340 $F.g^{-1}$	1M KOH	-	1.2
VN	[52]	850 $F.g^{-1}$	1M KOH	-	1.2
VN	[53]	2.5 $mF.cm^{-2}$	1M KOH	0.1 µm	0.6
TiN	[54]	26 $mF.cm^{-2}$	0.5M K_2SO_4	0.77 µm	0.7
TiN	[24]	35 $mF.cm^{-2}$	0.5M H_2SO_4	0.98 µm	0.8
CrN	[55]	15 $mF.cm^{-2}$	0.5M H_2SO_4	1.1 µm	0.8
CrN	[56]	40 $mF.cm^{-2}$	0.5M H_2SO_4	1.1 µm	0.8
TiN	[57]	69 $mF.cm^{-2}$	1M LiOH	4 µm	0.6
MoN	[57]	52 $mF.cm^{-2}$	1M LiOH	4 µm	0.6
TiN / MoN	[57]	121.5 $mF.cm^{-2}$	1M LiOH	4 µm	0.6
RuN	[23]	6 $mF.cm^{-2}$	1M KOH	0.45 µm	0.9
VN	[27]	225 $F.g^{-1}$	1M KOH	150 µm	1
TiN	[27]	150 $F.g^{-1}$	1M KOH	151 µm	1
VN / TiN	[27]	250 $F.g^{-1}$	1M KOH	152 µm	1
VN	[43]	19 $mF.cm^{-2}$	1M KOH	0.28 µm	0.6
VN / TiN	[58]	24 $mF.cm^{-2}$	1M KOH	0.24 µm	0.9
Nb_4N_5	[59]	220 $mF.cm^{-2}$	1M H_2SO_4	17.4 µm	0.6
MoN	[28]	55 $mF.cm^{-2}$	0.5M Li_2SO_4	0.75 µm	0.9
WN	[29]	*29 $F.g^{-1}$	5M LiCl	-	1
Mo-W-O-N	[32]	0.172 $mF.cm^{-2}$	1M H_2SO_4	-	0.8
VN-CNTF	[26]	600 $mF.cm^{-2}$	3M KOH	7.5 µm	
β-W_2N	[21]	0.060 $mF.cm^{-2}$	1M KOH	-	0.8
γ-Mo_2N	[21]	0.256 $mF.cm^{-2}$	0.1 M H_2SO_4	-	0.8
	[21]	0.223 $mF.cm^{-2}$	0.1M HBF_4	-	0.8
	[21]	0.092 $mF.cm^{-2}$	0.1M $[(C_2H_5)_4N]_2SO_4$	-	0.8
	[21]	0.259 $mF.cm^{-2}$	0.1M $[(C_2H_5)_4N]BF_4$	-	0.8
VN	[21]	0.615 $mF.cm^{-2}$	0.1M KOH	-	1.1
	[21]	0.171 $mF.cm^{-2}$	0.1M $K(CF_3SO_3)$	-	1.1

		^{2}			
	[21]	0.6 $mF.cm^{-2}$	0.1M $[(C_2H_5)_4N]OH$	-	1.1
	[21]	0.16 $mF.cm^{-2}$	0.1M $[(C_2H_5)_4N](CF_3SO_3)$	-	1.1
VN	[42]	220 $mF.cm^{-2}$	1M KOH	3.4 µm	0.6

The capacitances are given in $mF.cm^{-2}$ or $F.g^{-1}$ depending on the synthesis / deposition methods which lead to the synthesis of powder or thin films electrodes. " * " Estimated capacitance based on C = 5 $F.cm^{-3}$ and mass loading = 168 $mg.cm^{-3}$. " - " means that the thickness is unknown.

Table 1 – Overview of the transition metal nitride electrodes used for electrochemical capacitors or micro-supercapacitors

ACCEPTED MANUSCRIPT

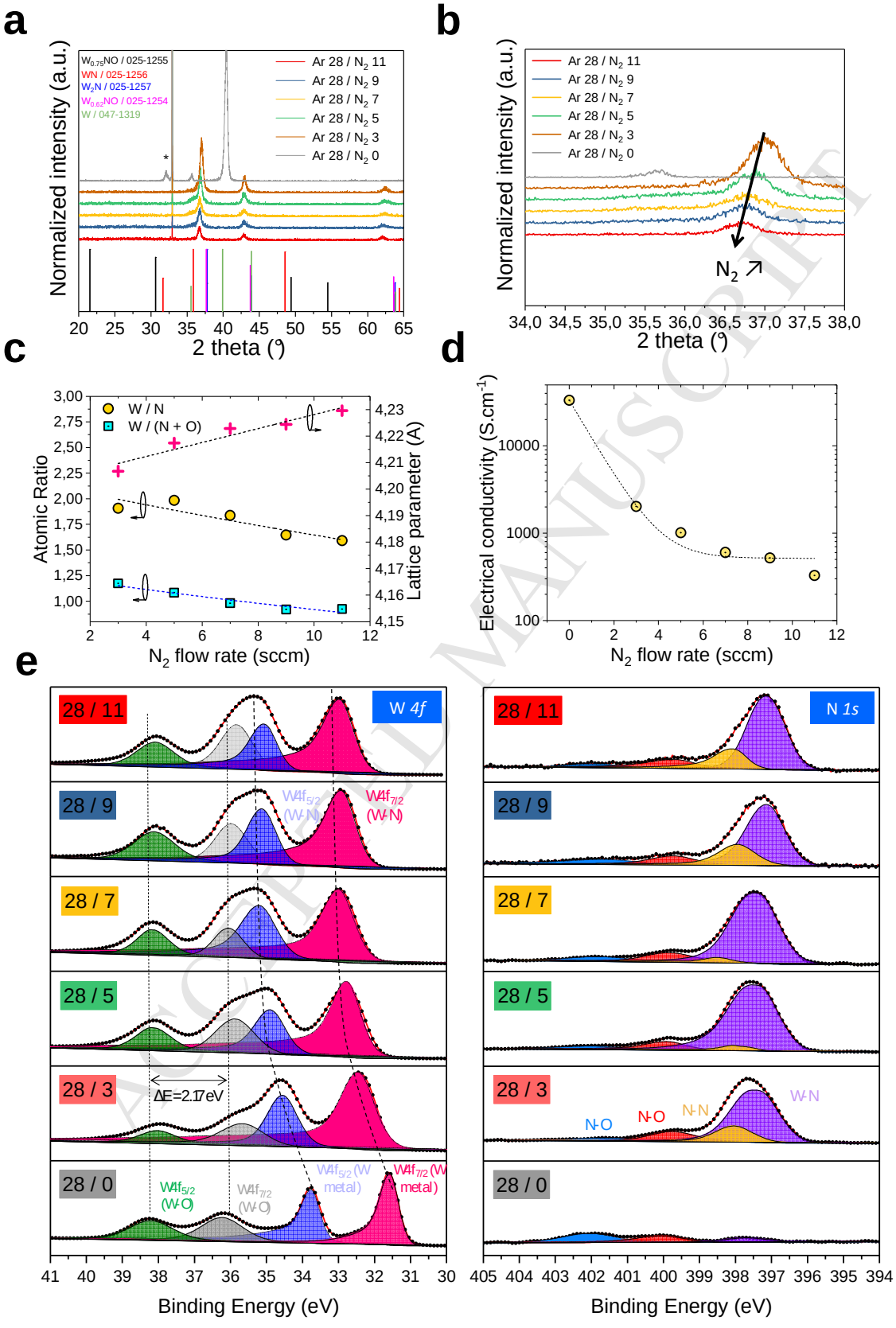

ACCEPTED MANUSCRIPT

Figure 1 – a/b. X-Ray diffraction analyses of the tungsten nitride thin films deposited at different N_2 flow rates. **c.** Evolution of the lattice parameter and the atomic ratio according to the nitrogen flow rate. The quantification of the elements is extracted from XPS spectra. **d.** Evolution of the film conductivity vs the N_2 flow rate. **e.** High resolution XPS core level spectra of the tungsten nitride films vs the concentration of nitrogen in the sputtering gas: focuses of the N *1s* and W *4f* core levels are highlighted. For a sake of clarity, the samples are numbered using the "28 / Y" format where 28 corresponds to the argon flow rate (28 sccm) used during the sputtering process and Y the N_2 flow rate (in sccm).

ACCEPTED MANUSCRIPT

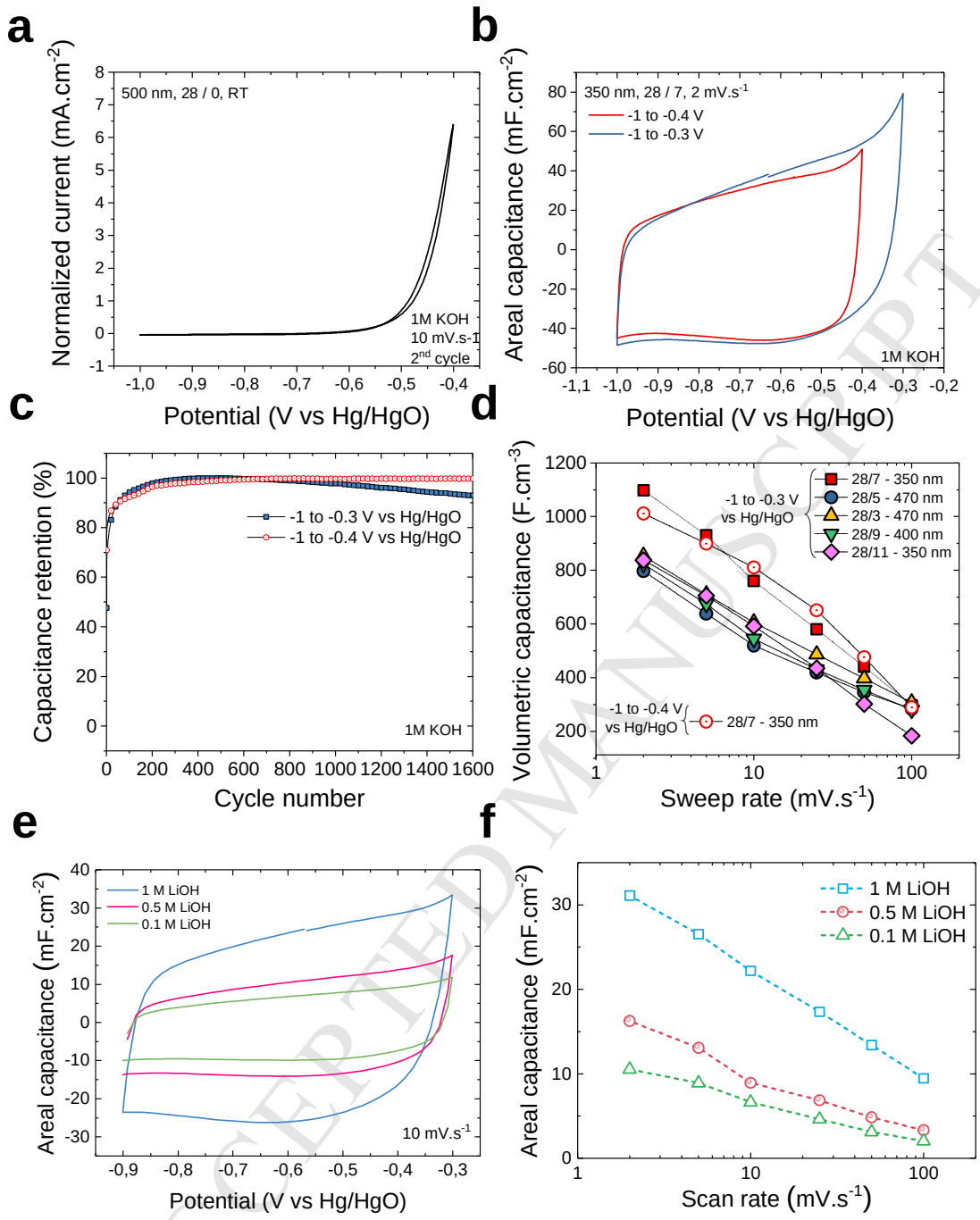

Figure 2 – Electrochemical analyses of the tungsten nitride films deposited at room temperature on Si / Si_3N_4 substrate. **a.** CV of the pure tungsten film measured in 1M KOH electrolyte at 10 $mV.s^{-1}$. **b.** CV of the sample deposited with N_2 = 7 sccm flow rate and tested in two different electrochemical windows. **c.** Evolution of the capacitance vs the number of cycles using two different electrochemical windows. **d.** Volumetric capacitance vs sweep rates and N_2 flow rates. **e.** CV of the best sample (deposited with N_2 flow rate = 7 sccm) tested in several concentration of LiOH aqueous electrolyte. **f.** Evolution of the

areal capacitance vs the scan rate in LiOH electrolyte. For a sake of clarity, the samples are numbered using the "28 / Y" format where 28 corresponds to the argon flow rate (28 sccm) used during the sputtering process and Y the N_2 flow rate (in sccm).

ACCEPTED MANUSCRIPT

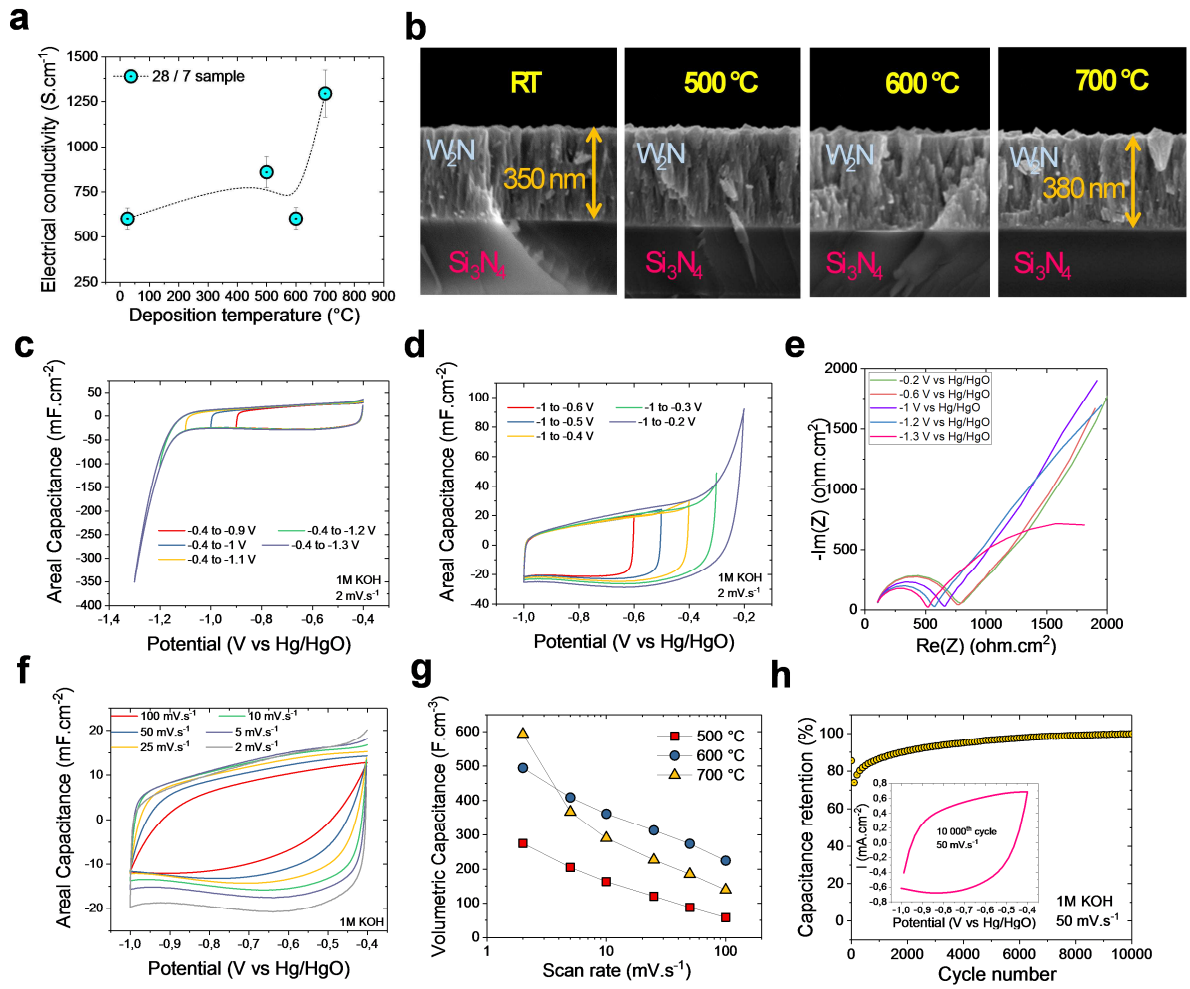

Figure 3 – Electrical and electrochemical performances of W_2N films deposited at high temperature. **a.** Plot of the electrical conductivity vs the deposition temperature. **b.** SEM morphologies of the four samples under test. **c. and d.** CVs of the sample deposited at 600 °C and tested in 1M KOH at 2 $mV.s^{-1}$ with various lower and upper cut-off potentials. **e.** Electrochemical impedance spectroscopy of the sample deposited at 600 °C. **f.** CVs in 1M KOH at different sweep rates. **g.** Volumetric capacitances vs the scan rate in 1M KOH electrolyte. For a sake of clarity, the samples are numbered using the "28 / Y" format where 28 corresponds to the argon flow rate (28 sccm) used during the sputtering process and Y the N_2 flow rate (in sccm). **h.** Capacitance retention as a function of the number of cycles in 1M KOH at 50 $mV.s^{-1}$ (10 000 cycles). An inset of the CV after 10 000 cycles is reported to demonstrate the good electrochemical performance of the sputtered W_2N films.

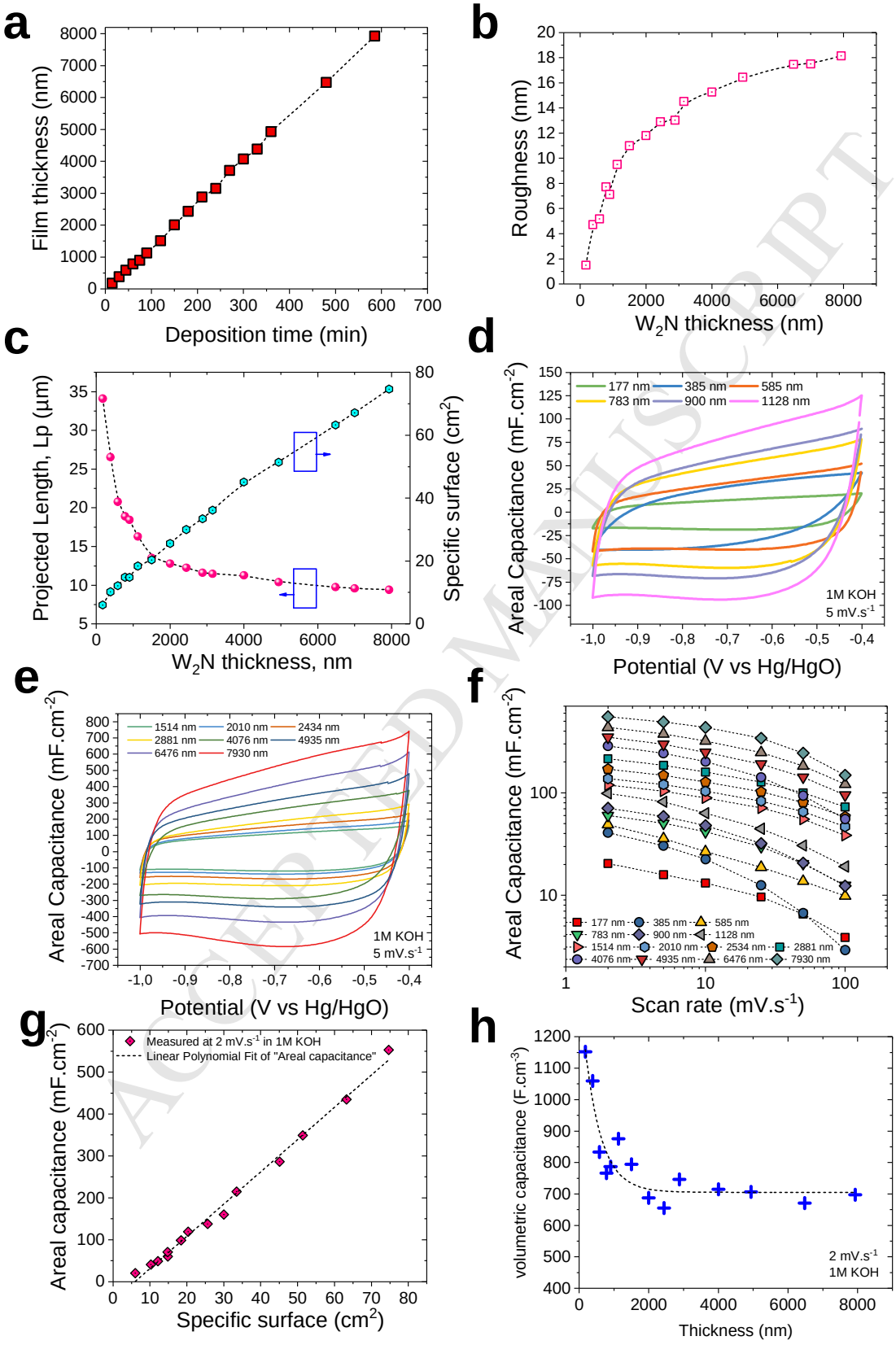

ACCEPTED MANUSCRIPT

Figure 4 – Evolution of W_2N performance vs film thickness. **a.** Film thickness measured by SEM vs deposition time. **b.** Plot of the roughness vs the W_2N thickness. **c.** Evolution of the specific surface and projected length vs the thickness. **d. and e.** CVs of various samples exhibiting different thickness measured at 5 $mV.s^{-1}$ in 1M KOH. **f.** Plots of the areal capacitance vs the sweep rate. **g.** Evolution of the areal capacitance extracted from electrochemical measurement vs the specific surface, extracted from AFM analyses. **h.** Volumetric capacitance of W_2N films vs the thickness.

ACCEPTED MANUSCRIPT

Supplementary materials

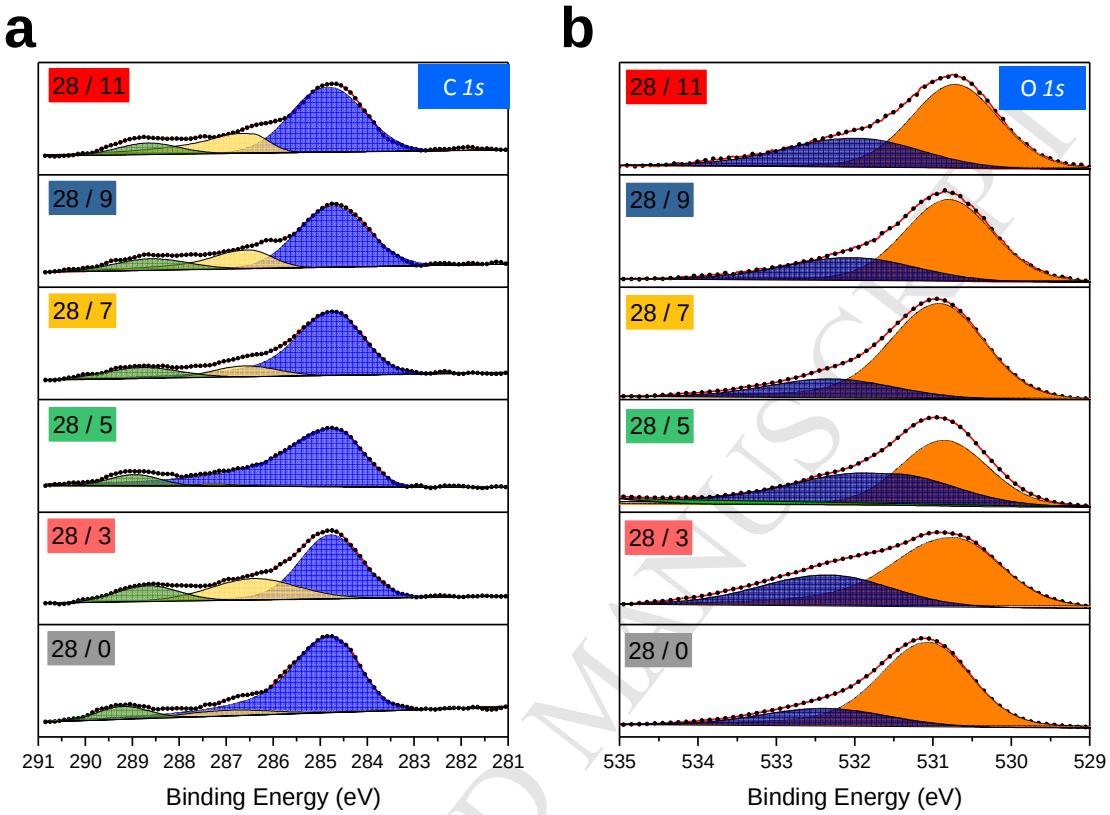

Figure SI1 – XPS core levels spectra of O *1s* and C *1s* of the sputtered tungsten nitride thin films vs the nitrogen flow rates. For a sake of clarity, the samples are numbered using the "28 / Y" format where 28 corresponds to the argon flow rate (28 sccm) used during the sputtering process and Y the N_2 flow rate (in sccm).

ACCEPTED MANUSCRIPT

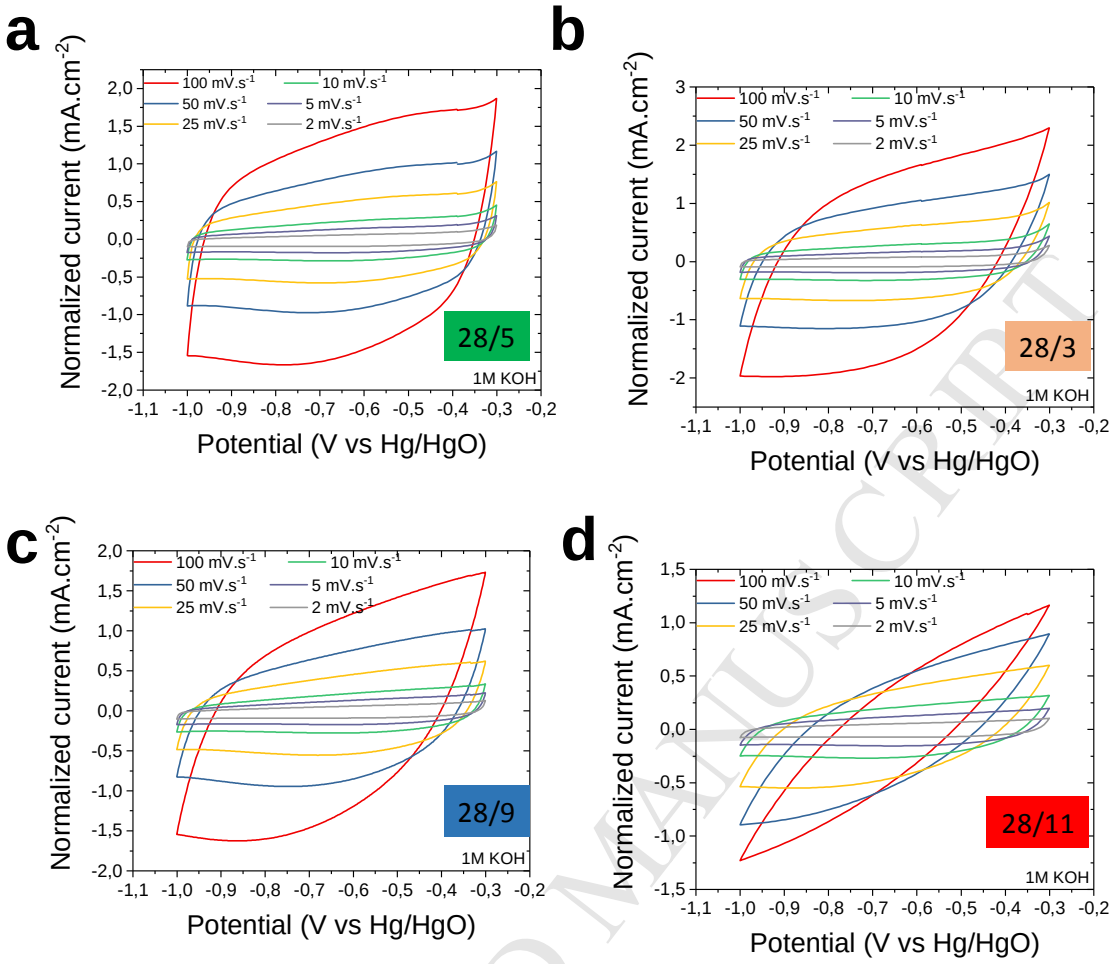

Figure SI2 – Electrochemical analysis of four samples deposited at room temperature with various nitrogen flow rates. For a sake of clarity, the samples are numbered using the "28 / Y" format where 28 corresponds to the argon flow rate (28 sccm) used during the sputtering process and Y the N_2 flow rate (in sccm).

ACCEPTED MANUSCRIPT

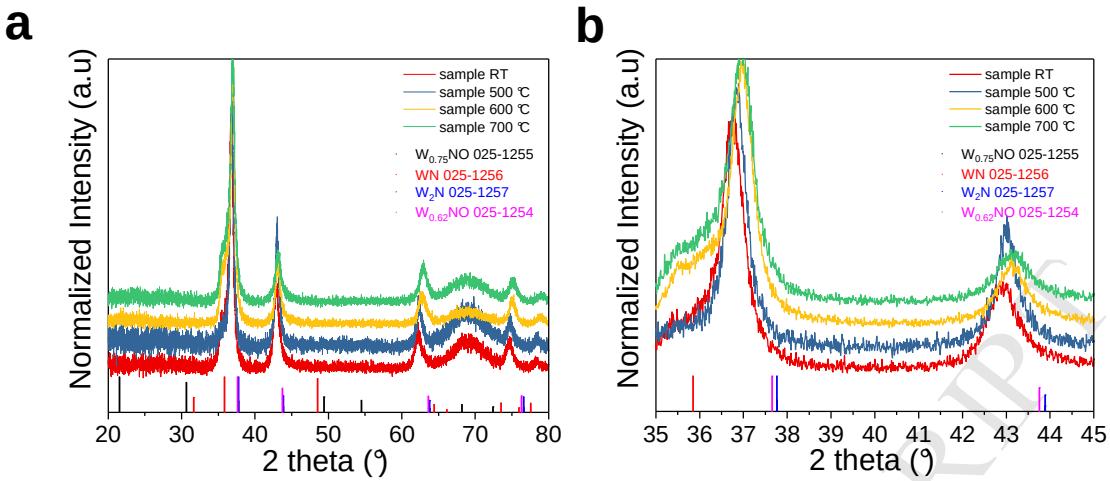

Figure SI3 – X-ray diffractogramms of W_2N samples deposited at RT, 500, 600 and 700 °C respectively.

ACCEPTED MANUSCRIPT

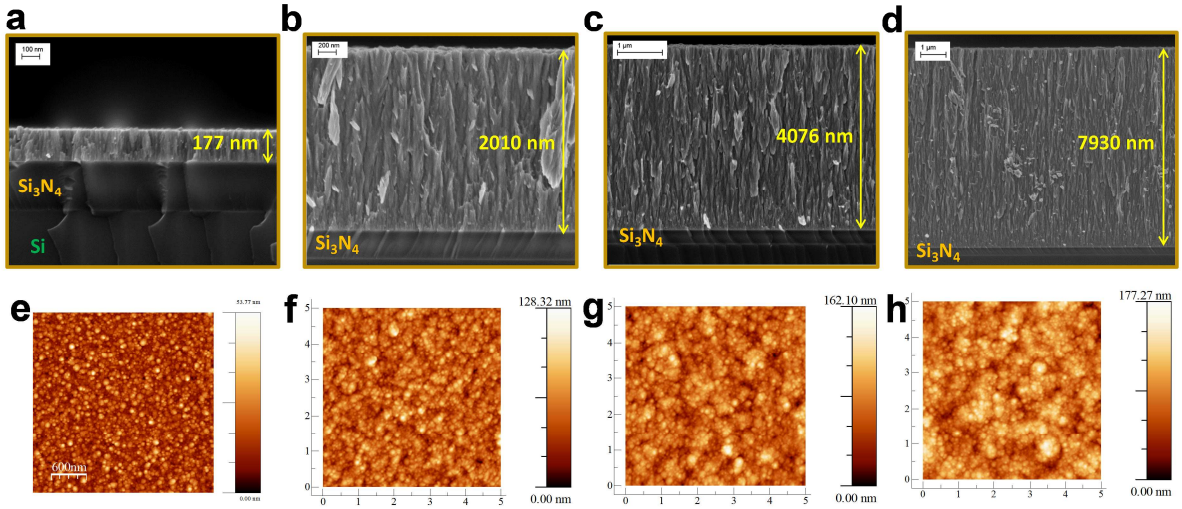

Figure SI4 - SEM cross sections (a-d) and top view AFM analyses (e-h) of various W_2N samples with different thicknesses.

Determination of the projected length

In the following part, we illustrate the way we determine the projected length. A 3.15 µm-thick sample is used as an example (scanning area = 25 μm^2, i.e. 5 x 5 μm^2). The images and the projected length are obtained using the free software Gwyddion.

We start from the scanning AFM image (**Figure SI5**).

In order to increase the selectivity of the analysis, we transform z to z^2 (**Figure SI6**). This operation does not change the base of the grain but only their height are changed, which does not matter for the analysis.

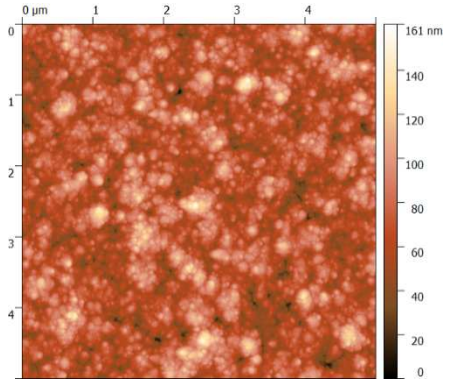

Figure SI5 - AFM image, 5 µm x 5 µm

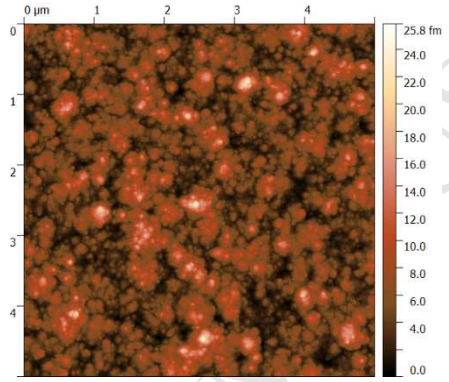

Figure SI6 - Square of the image

Thus, we apply a mask to the image (defined with a given percentage of the height, the so called mask threshold) This mask selects a fraction of the grains, by moving the z position of an horizontal plane on which the selected grains are projected. The projection is the so-called projected length. As illustrated in the table SI1-, we search the maximum for the projected length by tuning the threshold.

Mask Threshold (%)	Illustration of the selected grains	Projected length (microns)

16	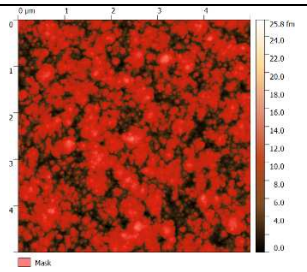	284.3
18	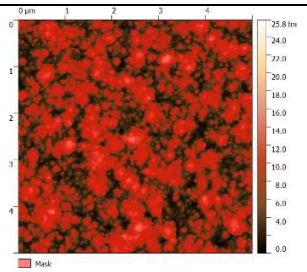	289.5
20	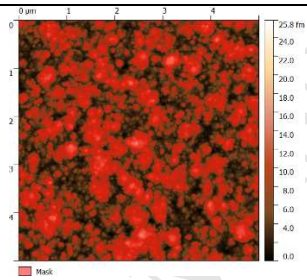	273

Table SI1 - Procedure used to determine the projected length

The variation of the projected length versus the threshold is given in the **figure SI7**.

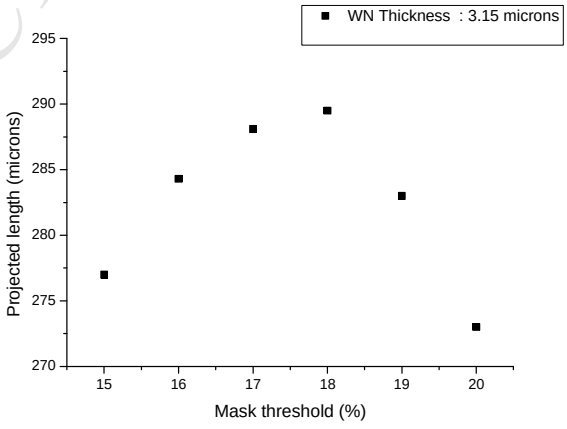

Figure SI7 - Variation of the projected length versus the threshold

From this procedure, we deduce that the maximum length is equal to 289.5 µm, for an area of 25 μm^2 , i.e. a value of 11.58 µm for a one micron square. This analysis is repeated for different image sizes and at different spots on the surface, leading to an average value determined over 12 measurements.

ACCEPTED MANUSCRIPT